



Full length article



Fundamental study to grow single crystals with high performances operated up to high temperatures in donor-doped materials for energy harvesting

Su-Jin Ha^{a,b}, Young Kook Moon^a, Hyun-Ae Cha^a, Jong-Jin Choi^a, Byung-Dong Hahn^{a,*}, Seong-Hui Choi^b, Il-Ryeol Yoo^b, Kyung-Hoon Cho^{b,*}, Kyoung-Seok Moon^c, Cheol-Woo Ahn^{a,*}

^a Functional Ceramics Department, Powder & Ceramics Division, Korea Institute of Materials Science (KIMS), Changwon, Gyeongnam 641-831, Republic of Korea

^b School of Materials Science and Engineering, Kumoh National Institute of Technology, 61 Daehak-ro, Gumi, Gyeongbuk 39177, Republic of Korea

^c School of Materials Science and Engineering, Gyeongsang National University, Jinju, Gyeongnam 52828, Republic of Korea

ARTICLE INFO

Keywords:

Energy harvesting
Donor doping
Pb-free material
Single crystal Seed particle

ABSTRACT

An energy-harvesting material with high energy-conversion constant ($d_{33} \times g_{33}$) and Curie temperature (T_C) is required to effectively harvest the mechanical energy which has not been recycled into electrical energy. Here, we present an eco-friendly single-crystals, the 3rd generation material, for energy harvesting with the excellent $d_{33} \times g_{33}$ of $118 \times 10^{-12} \text{ m}^2 \text{ N}^{-1}$ ($d_{33}=1030 \text{ pC N}^{-1}$) and high T_C of $390 \text{ }^\circ\text{C}$, prepared by simple heat-treatment. A donor (not an acceptor) has been doped to (K,Na)NbO₃ (KNN)-based materials to obtain single-crystals through exceptionally abnormal grain growth (AGG). The severe AGG in a donor-doped KNN is explained by the donor effect to locally accelerate the volatilization of metals earlier. In particular, a donor-doped PbTiO₃ (PT + Bi³⁺) material as well as a donor-doped KNN material allows for the synthesis of a single-crystal seed through the simple molten salt method. These findings advance understanding of sintering mechanisms in metal-volatile oxides and offer significant progress in energy-harvesting materials.

1. Introduction

Energy harvesting has become a growing priority to conserve the earth's environment, and the various types of energies such as light, heat, and mechanical energy are being converted into electric energy and then stored or used [1–7]. In our daily lives, the mechanical energy is constantly generated through a wide variety of activities, such as the walking of people and the movement of cars, but it is rarely converted into electricity. In order to harvest the mechanical energy and effectively convert to electrical energy, a variety of studies have been conducted to develop the material which has a high conversion performance ($d_{33} \times g_{33}$) [7,8]. d_{33} is piezoelectric constant and g_{33} is piezoelectric voltage constant [9,10]. They have the following relationship:

$$g_{33} = \frac{d_{33}}{\epsilon_{33}^T} \quad (1)$$

where ϵ_{33}^T is the dielectric constant under constant stress. For the high $d_{33} \times g_{33}$, the grain boundaries and pores should be minimized, and therefore a single-crystal material is generally preferable to a polycrystalline material. In addition, a material with a low dielectric

constant is beneficial since g_{33} is high when the dielectric constant is low. Therefore, an excellent $d_{33} \times g_{33}$ can be predicted by growing huge grains of the energy conversion material which has a low dielectric constant. Furthermore, Energy harvesting materials must have a high Curie temperature (T_C), since energy harvesting devices generate a lot of heat during operation and energy harvesting materials lose their performance at the temperature above T_C . Pb(Zr,Ti)O₃ (PZT) ceramics which are commercial materials are widely used owing to their high piezoelectric constants, but they have low T_C of $150\text{--}350 \text{ }^\circ\text{C}$ [11–13]. On the other hand, PbTiO₃ (PT) shows high T_C of $>400 \text{ }^\circ\text{C}$ [14,15]. Moreover, the (K,Na)NbO₃ (KNN)-based ceramic has not only a high T_C of approximately $400 \text{ }^\circ\text{C}$, but also a low dielectric constant [16,17]. In addition, since KNN-based ceramics shows high $d_{33} \times g_{33}$ when phase transition temperature (T_{O-T}) from tetragonal structure (T) to orthorhombic structure (O) is near room temperature (RT), in this study, the T_{O-T} has been controlled to obtain high $d_{33} \times g_{33}$ in KNN-based ceramics [18–20]. In particular, huge grains which ensure an excellent $d_{33} \times g_{33}$ can be grown by simple sintering in donor-doped KNN ceramics which are chosen in this study. Here, a donor is an additive which has a higher valence, and thus it is the opposite of acceptor. In this study, we present

* Corresponding authors.

E-mail addresses: cera72@kims.re.kr (B.-D. Hahn), khcho@kumoh.ac.kr (K.-H. Cho), cheoruahn@kims.re.kr (C.-W. Ahn).

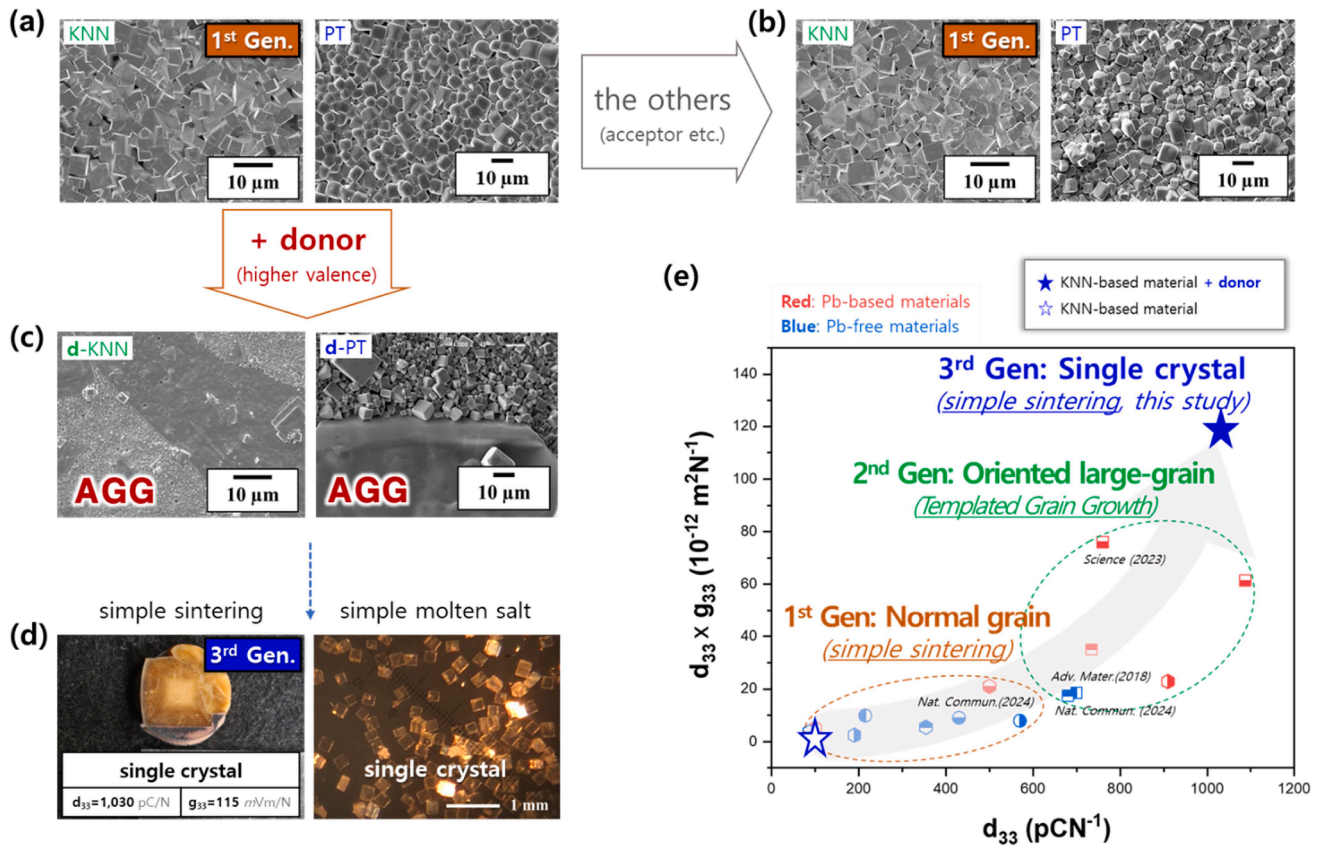


Fig. 1. Single-crystal materials grown by simple heat-treatment in donor-doped ceramics: SEM images of (a) KNN and PT and (b) KNN + Li⁺ (same valence) and PT + Fe³⁺ (acceptor) specimens, (c) SEM images of d-KNN and d-PT samples to show abnormal grain growth (AGG), (d) Single-crystal specimens grown by simple sintering and simple molten salt method (SMM), and (e) Development of energy-harvesting material from 1st to 3rd generation.

the fundamental studies that identify the mechanism that allows single crystal materials to be grown by simple heat treatment.

Large particles with a controlled shape have been widely investigated as the next-generation materials for energy harvesting, since they are used as the seeds for templated grain growth (TGG) to enhance $d_{33} \times g_{33}$ [21–25]. Moreover, they are also frequently compounded with polymers to develop a flexible device for energy harvesting [2,3,26–28]. The seeds are typically polycrystalline materials, and they are primarily prepared by topochemical reactions (TR) [29–31]. However, TR is not industry-friendly, and the polycrystalline materials need to be improved to single-crystal materials. We have demonstrated that single-crystal seeds can be prepared by simple molten salt method (SMS) which is industry-friendly, in not only donor-doped KNN (d-KNN) but also donor-doped PbTiO₃ (d-PT).

2. Experimental

“KNN and (K_{0.5}Na_{0.5}Bi_{0.005})NbO₃ (d-KNN, donor: Bi³⁺)”, (K_{0.475}Na_{0.475}Li_{0.08}Bi_{0.0025})(Nb_{0.97}Sb_{0.03})O₃ + 0.2 at. % MnO₂ (d-KNLNSM, donor: Bi³⁺), “PT and (PbBi_{0.06})TiO₃ (d-PT, donor: Bi³⁺)”, and “BaTiO₃ (BT) and Ba(TiNb_{0.005})O₃ (d-BT, donor: Nb⁵⁺)” were synthesized by the conventional solid-state route. The powders of K₂CO₃, Na₂CO₃, Li₂CO₃, Nb₂O₅, Sb₂O₃, MnO₂, Bi₂O₃, PbO, BaCO₃, TiO₂ (99.9 %, all obtained from Sigma Aldrich) were mixed for 24 h in a polypropylene jar with zirconia balls. The mixtures of powders were dried at 80 °C and calcined at 850–1000 °C (KNN and d-KNN: 900 °C, PT and d-PT: 850 °C, and BT: 1000 °C) for 3 h. The calcined powders were milled for 24 h, dried and pressed into disks under the pressure of 100 MPa and sintered at 1020–1300 °C (KNN and d-KNN: 1020–1100 °C, PT and d-PT: 1100 °C, and BT and d-BT: 1300 °C).

For the synthesis of single-crystal seeds, a molten salt method was

employed. The calcined powders of d-KNN and d-PT (CPKNN and CPPT) were combined with KF (99 %, Sigma-Aldrich) salt in a 0.5:0.5 CPKNN-to-KF and a 0.3:0.7 CPPT-to-KF weight ratio using a mixer. These mixtures were heated to 900 °C and 860 °C at a rate of 5 °C/min, held for 2 h, and then gradually cooled to 25 °C at a rate of 0.5 °C/min. The final products were washed repeatedly with HCl and deionized water to selectively remove the KF salt through filtration. Furthermore, the BT and BZT seeds were synthesized by the two-step process of TC reaction [22].

2.1. Analyses of microstructure and crystal structure

The crystal structures of the sintered specimens were determined through X-ray diffraction (XRD, Rigaku, D/MAX-500VL/PC) using Cu K α radiation ($\lambda=0.1542 \text{ nm}$). The microstructures of the samples were observed using a scanning electron microscope (SEM, JSM-6610LV; JEOL Ltd., Japan) and transmission electron microscope (TEM, JEM-2100F, JEOL Ltd., Japan). MD was calculated with TEM results.

2.2. Property measurement

The densities (ρ) of the specimens were measured using Archimedes’ method with *m*-xylene as the medium. The samples were poled in silicone oil at 120 °C by applying a DC field of 1 kV/mm for 30 min. All of the electrical measurements were conducted after aging the samples for 24 h. The piezoelectric and dielectric properties were determined using a piezo d_{33} meter (Micro-Epsilon Channel Product DT-3300) and an impedance analyzer (4294A, Agilent Technologies, Santa Clara, CA, USA). Permittivities as a function of temperature were obtained by measuring the capacitance and loss using an LCR meter (HP model 4284) in a furnace interfaced with a computer for data acquisition.

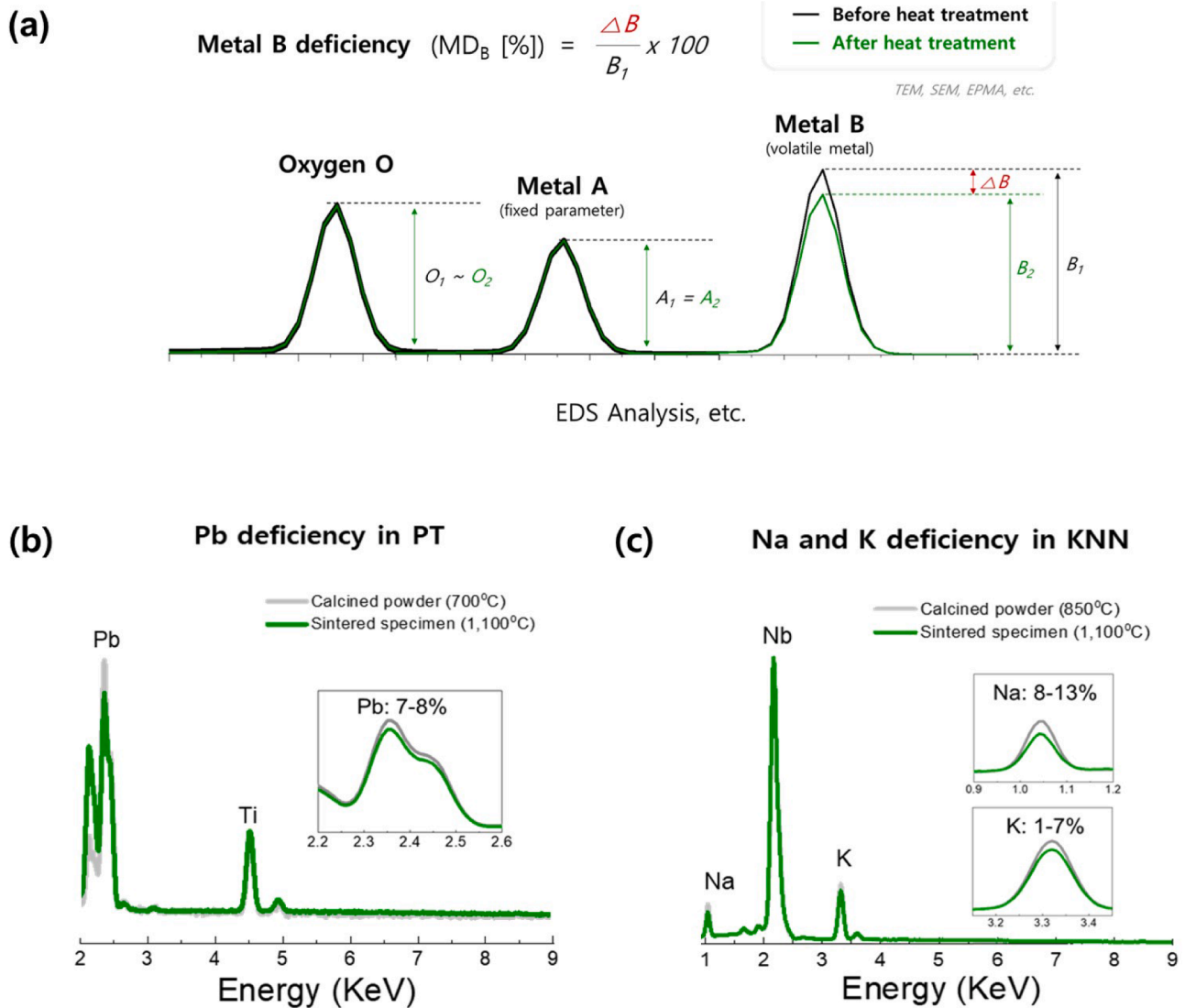


Fig. 2. Metal deficiencies (MDs) calculated with modified peak-intensities in (a) metal-volatile oxides, (b) PT, and (c) KNN. MD refers to the reduction ratio of a metal element due to the high-temperature heat treatment in a metal-volatile oxide (MVO), compared to the unheated specimen. To calculate the MD, the various analyses (such as TEM, SEM, EPMA etc.) can be used. In KNN and PT, they were analyzed using TEM. Nb and Ti do not show the difference in the intensity of an EDS peak. The Nb and Ti peaks were used for the fixed parameters to be compared to K & Na and Pb.

2.3. Thermogravimetry (TG)

TG (STA 409 PC, NETZSCH, Germany) was performed to determine the temperature at which the liquid phase forms in PT and the temperature at which Pb volatilizes in PT. The temperature increase rate was $5\text{ }^\circ\text{C min}^{-1}$, and heating was performed from 20 to $1400\text{ }^\circ\text{C}$.

3. Result and discussion

3.1. 3rd generation material for energy harvesting

The KNN and PbTiO_3 (PT) ceramics shown in Fig. 1(a) are piezoelectric materials which have been studied for energy harvesting materials, and they exhibit the typical microstructure of a sintered specimen. As indicated in Fig. 1(c), this normal microstructure changes to a microstructure in which abnormally grown grains are observed when the donor is added, while no change in microstructure is observed when the others are added, as shown in Fig. 1(b).

In general, the normal-grain materials (NG) do not have high $d_{33} \times g_{33}$ or piezoelectric constant (d_{33}), as seen in the 1st generation material

of Fig. 1(e). Recently, thus, various studies have been conducted to develop the oriented large-grain materials (OLG, TGG: templated grain growth, the 2nd generation) which show the higher performances of $d_{33} \times g_{33}$ and d_{33} for energy harvesting than NG. In OLG, the grain size is large and thus the energy harvesting property is relatively high due to the lower degradation caused by grain boundaries. In addition, the higher performance is expected since the crystal structure is oriented.

Single-crystal materials (SC) have much higher properties, since SC does not have the grain boundary. Nevertheless, SC has not been widely used in industry due to the high cost of the processes such as Bridgman method and self-flux method. Therefore, as shown in Fig. 1(a and c-d), SC manufactured by conventional ceramic processes is definitely the 3rd generation material for energy harvesting. In particular, the single-crystal seeds [right image of Fig. 1(d)] can be used as seed particles, an essential material for OLG fabrication, and can be composited with polymers to prepare flexible energy-harvesting devices. In addition, the single-crystal materials of Fig. 1(c-d) and S1 have the scientific significance, as they are only grown in the addition of a donor (d-KNN and d-PT) among the various additives.

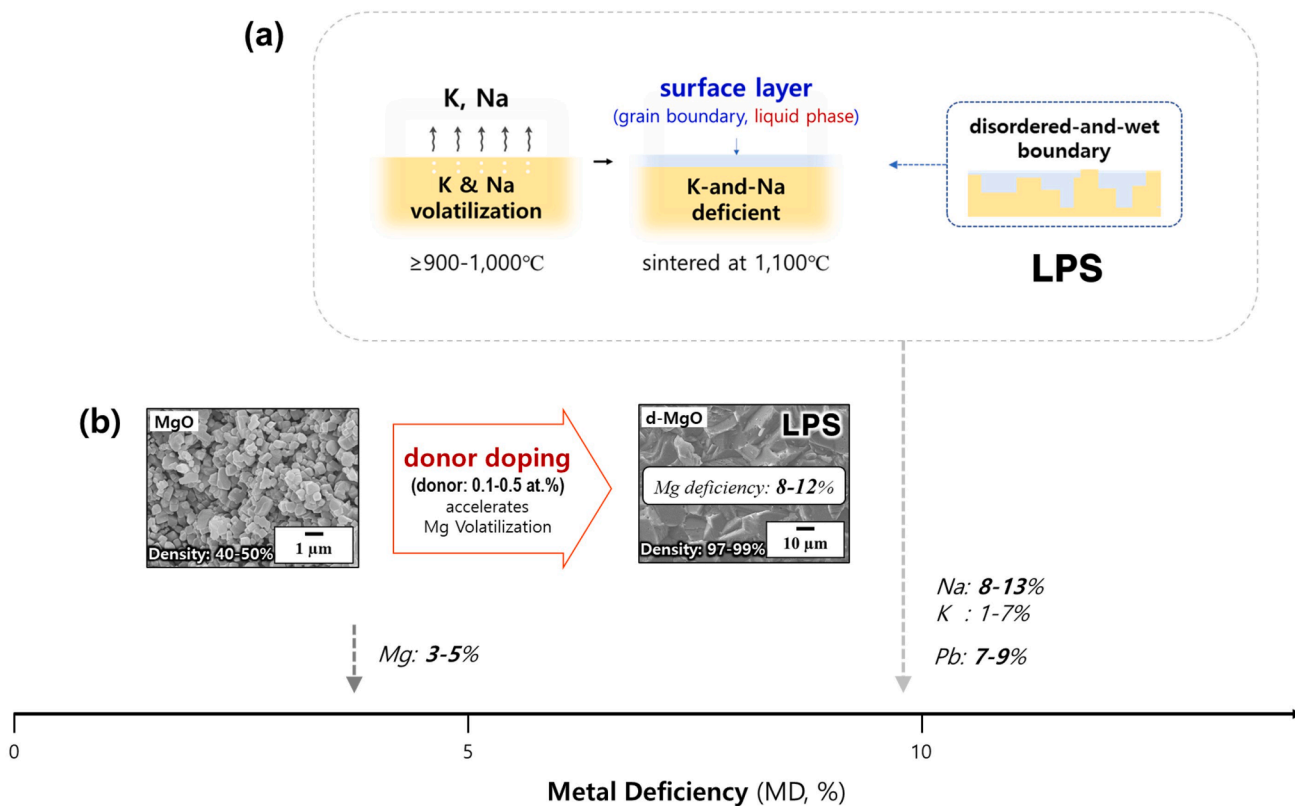


Fig. 3. Schematic diagram describing LPS by metal volatilization (MV): (a) schematic diagram of liquid-phase formed on surface of KNN particle due to MV. In the sintering behavior, the critical driving force is decreased by changing the disordered interface structure. (b) Donor-doping effect in MgO.

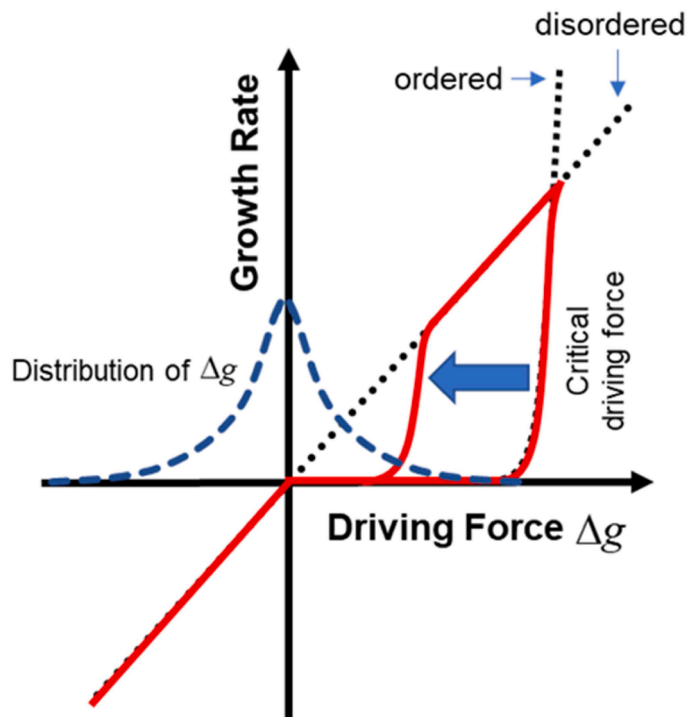


Fig. 4. Schematic representation showing crystal growth rate as a function of driving force for diffusion (dashed line) and mixed (diffusion and interface reaction) control (solid lines) mechanism.

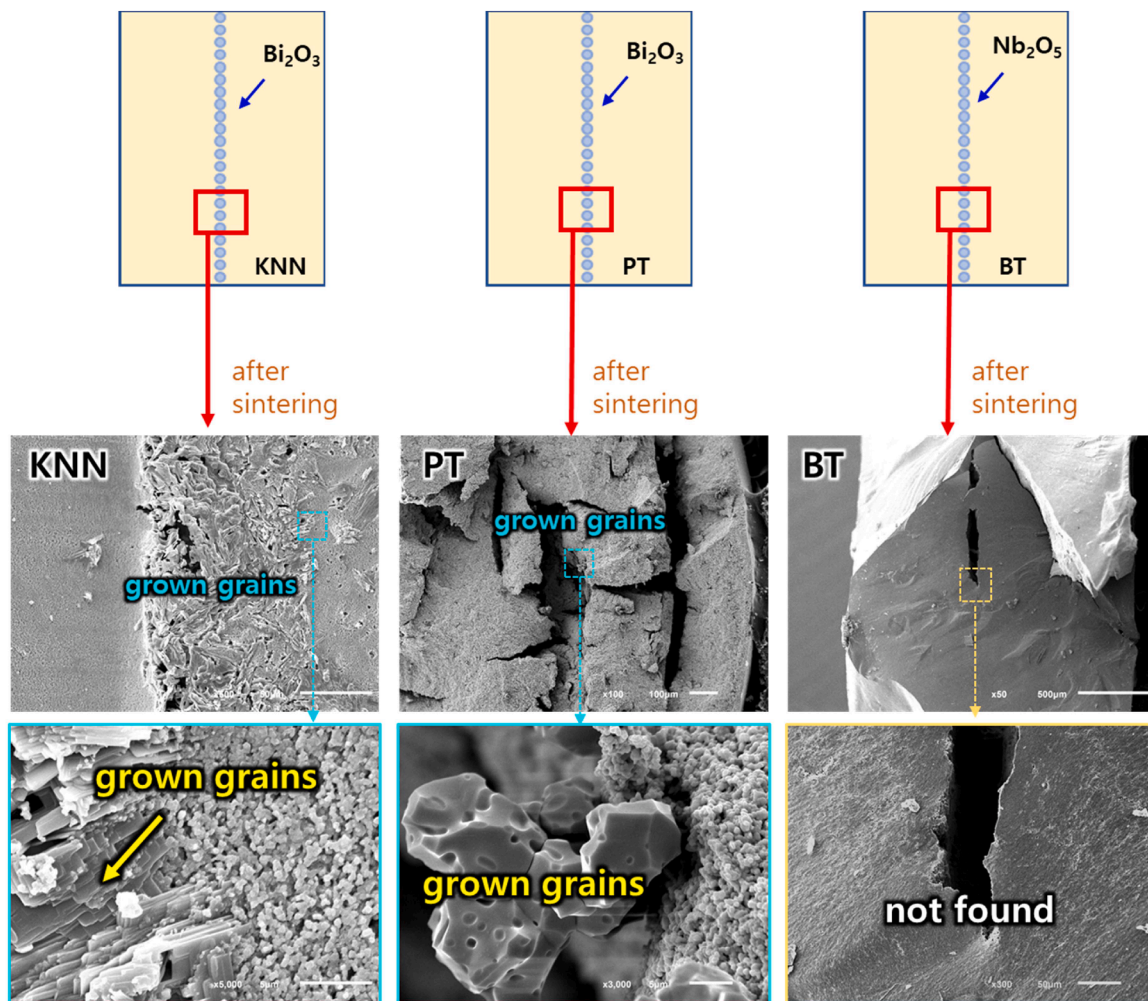


Fig. 5. SEM images of KNN, PT, and BT to show local differences and AGG. A thin layer of donor powder was formed between the thick layers of KNN (or PT, or BT) powders, and then the specimens were sintered. In KNN and PT, Bi^{3+} was used as the donor, while Nb^{5+} was used in BT. After sintering each specimen, the microstructure was observed by SEM images. Grain growth and densification occurred only in the range of donor powder in KNN and PT.

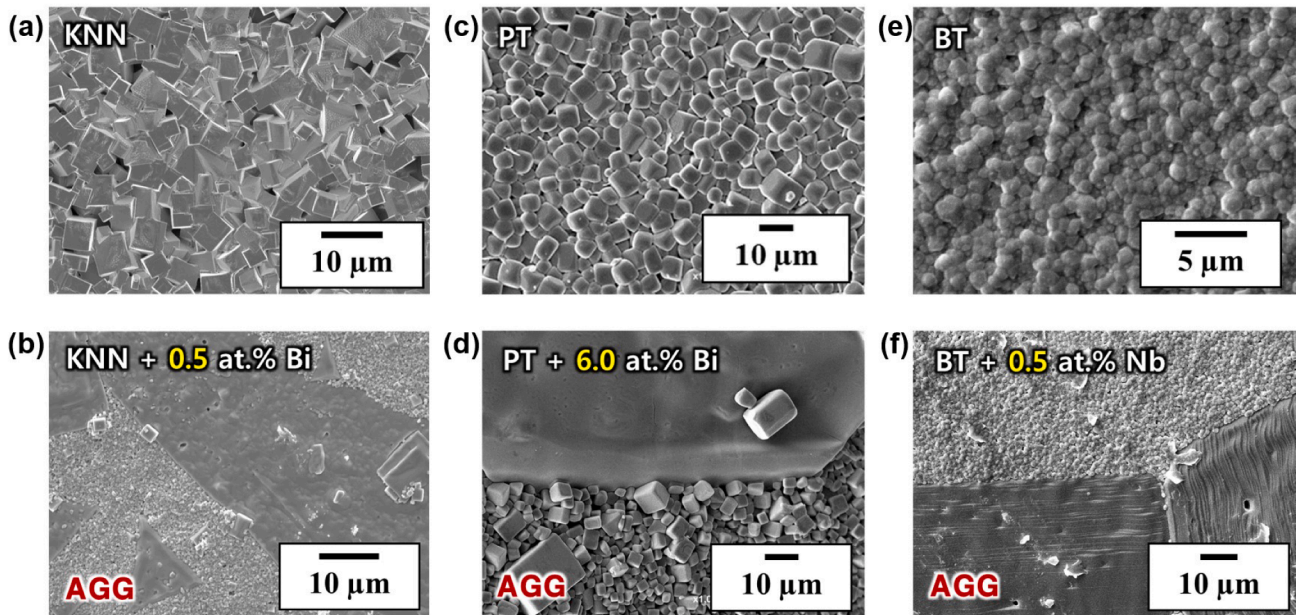


Fig. 6. SEM images to show AGG caused by donor-doping in (a) KNN, (b) PT, and (c) BT. A relatively large amount of donors (3.0–7.0 at. %) are required in PT, compared to KNN (0.3–0.9 at. %) and BT (0.3–0.7 at. %).

3.2. Crystal growth behavior in *D*-KNN & *D*-PT

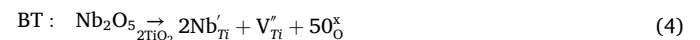
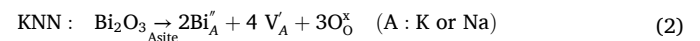
In general, liquid-phase sintering (LPS) is observed in the sintering behavior of KNN and PT, and the elements of K, Na, and Pb are volatile at the sintering temperature of approximately 1100 °C [32–37]. Hence, the effect of the metal volatilization (MV) on LPS was investigated in this study, initially. Indeed, a weight loss does occur when they are heat-treated at high temperatures of >900 °C, as shown in Fig. S2. To clarify the MV, metal deficiency (MD) was devised to verify MV differences, as indicated in Fig. 2(a). MD quantifies the reduction in metal content following high-temperature heat treatment, characterized through scanning electron microscope (SEM), transmission electron microscope (TEM), electron probe microanalysis (EPMA), etc. Figs. 2 (b-c) show the MD extent of Na and Pb (approximately 7–13 %) resulting from MV in KNN and PT. Details on MD calculation are provided in Table S1 and Fig. S3. MD of 7–13 % in KNN and PT does not imply that this percentage of metals was volatilized during sintering; rather, it indicates a significant decrease in the proportion of these metals compared to Nb and Ti which are not volatile elements.

SEM images of KNN and PT sintered at 1100 °C are shown in the LPS images of Fig. 1(a). The images show dense microstructures (relative density: >98 %) formed via LPS [38,39]. The liquid phase formed in KNN is not presented in this manuscript, as it has been reported previously [36,37]. As depicted in the process schematic of Fig. 3(a), liquid-phase formed on particle surfaces likely results from significant MV (K, Na, and Pb). The liquid phase formation at grain boundaries in polycrystalline materials can be attributed to the segregation or non-uniformity of elements at the boundaries [40,41]. When liquid phase is formed at grain boundaries, it accelerates elemental diffusion during sintering, thereby increasing the velocity of interface migration.

Numerous studies have reported the interplay between grain-growth behavior and interface structure in polycrystalline materials [34,35,41, 42]. The behavior of grain growth is influenced by the diffusion and reactions at interfaces, making interface structure a crucial factor in controlling grain growth. Atomically disordered interfaces provide numerous nucleation sites, such as kink sites, where atoms can attach without expending energy [43,44]. Consequently, the growth behavior is primarily diffusion-controlled, with the growth rate directly proportional to the driving force. In such a scenario, nearly all grains can grow,

resulting in normal grain-growth behavior. Conversely, atomically ordered interfaces facilitate two-dimensional nucleation and the attachment of lateral growth and interface defects like screw dislocations and twins [35,43]. At atomically-ordered interfaces, grain growth is influenced by a mixed control of interfacial reactions and diffusion, where grain growth occurs only when the driving force exceeds a critical value (referred to as the critical driving force for growth). Therefore, normal grain-growth behavior can be restored as the critical driving force decreases, characteristics of AGG systems. Conversely, systems exhibiting normal grain growth can show apparent AGG with an increase in the critical driving force. Fig. 4 shows a schematic representation illustrating the growth rate of a grain as a function of the driving force for diffusion and control mechanisms under the two-dimensional nucleation and growth.

In KNN and PT, a Bi^{3+} ion can enter the sites of a K^+ ion, a Na^+ ion, and a Pb^{2+} ion, and thus it is a donor in KNN and PT. In similar, a Nb^{5+} ion is a donor in BaTiO_3 (BT) since it can enter the site of a Ti^{4+} ion. Doping the donor in KNN, PT and BT, metal vacancies are formed as follows;



In the *D*-KNN and *D*-PT samples, a limited number of grains exhibited significant growth [45,46]. In fact, the interface structures in *D*-KNN and *D*-PT can be engineered to introduce slight atomic disorder through accelerated Na-volatilization or the enhanced Pb-deficiency [Eqs. (1)-(2)] using donor doping. Consequently, AGG in *D*-KNN and *D*-PT can be attributed to a reduction in the critical driving force for growth, allowing early growth of a few grains. When the volatilization does not occur, the critical driving force remains high, inhibiting widespread grain growth. However, due to MV, the critical driving force decreases, allowing only small portion of grains to grow, thus leading to AGG, as indicated in Fig. 4.

In general, this mechanism which is explained above is considered to understand the sintering behavior of a ceramic material, but it is not an

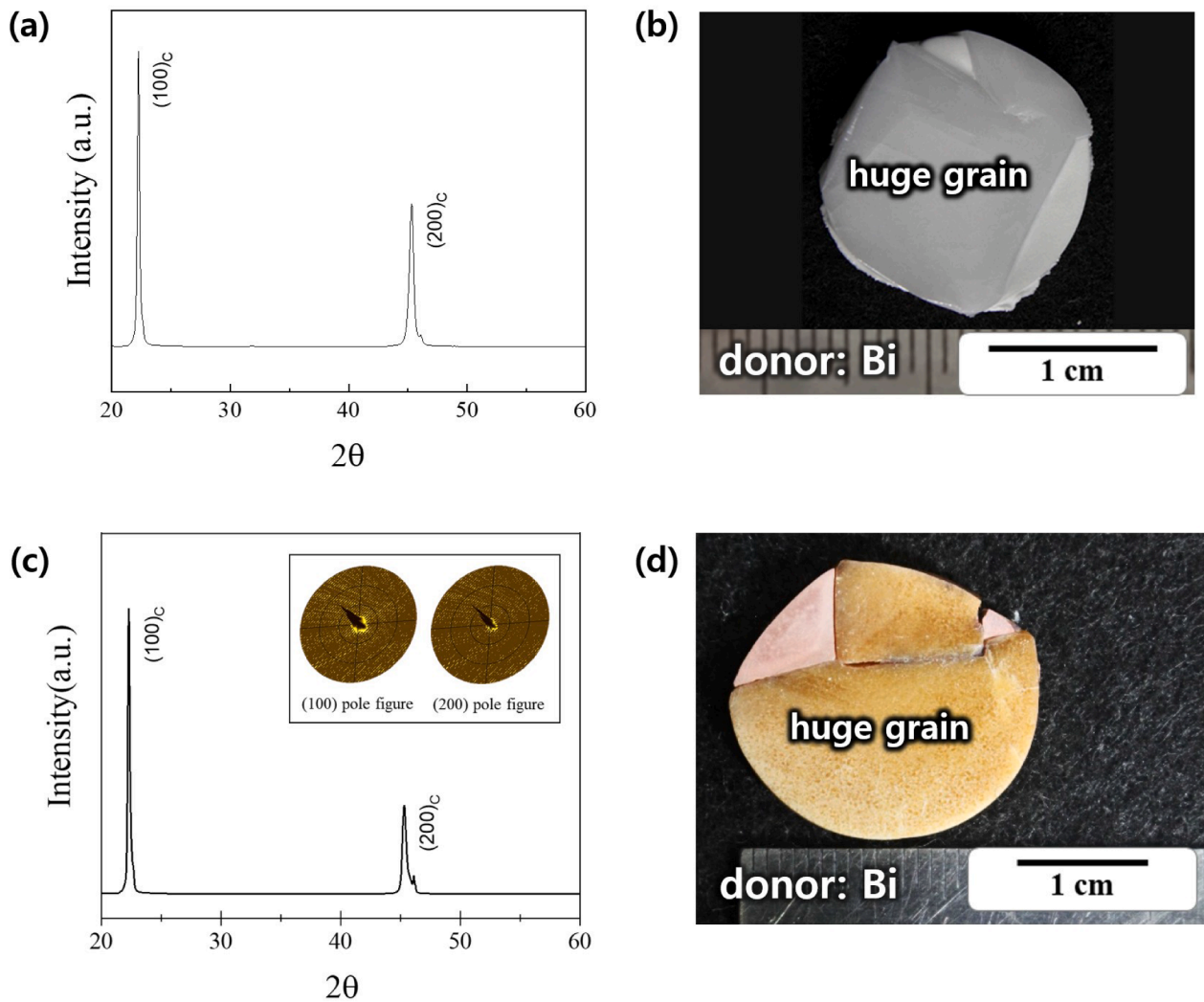


Fig. 7. X-ray diffraction (XRD) patterns and photographs in *d*-KNN ceramics: (a-b) huge grains of sintered specimens in $(\text{K,Na,Li})(\text{Sb,Nb})\text{O}_3 + 0.25 \text{ at. } \% \text{ Bi}^{3+}$ (*d*-KNLNS, donor: Bi^{3+}), (c-d) Huge grains of sintered specimens in *d*-KNLNSM. They show huge grains of cm-scale in size and orthorhombic and tetragonal phase are coexisted at room temperature.

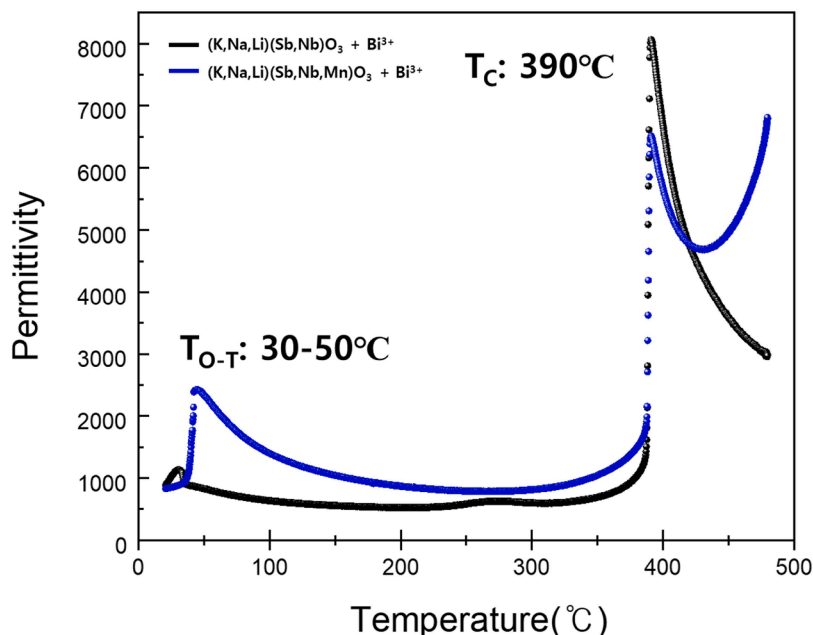


Fig. 8. Variation of permittivities with temperature in huge grains of $(\text{K,Na,Li})(\text{Nb,Sb})\text{O}_3 + \text{Bi}^{3+}$ (d-KNLNS) and d-KNLNSM specimens.

easy approach for readers. Therefore, in this study, we suggest an easy approach to describe the sintering behavior observed in metal-volatile oxides. As described in Fig 3(a), it is the sintering behavior predicted by the variation of the particle surface with metal volatilization.

In d-PT and d-KNN, AGG can be explained by the local differences, as shown in Figs. 5 and S4–5. The donor is concentrated on the center line in the specimens of Figs. 5 and S5, and the grain growth is localized in the donor area of KNN and PT. Namely, in d-KNN and d-PT, significant grain growths occur earlier in the region where the donor is located, as indicated in Figs. 5 and S4. This observation is consistent with Eqs. (1)–(2); the donor doping is expected to increase metal vacancies, potentially contributing to the AGG in metal-volatile oxides (MVOs) of d-KNN and d-PT. On the contrary, this localized-donor effect has not been observed in BT, a non-MVO, as seen in the right images of Fig. 5. Nevertheless, as seen in Fig. 6, AGG occurs in donor-doped BT (d-BT). Hence, AGG of d-BT may differ from that of d-KNN and d-PT induced by localized donors in MVOs.

Furthermore, there were significant differences in donor concentrations between d-KNN and d-PT, both of which exhibit AGG, as indicated in Fig. 6. In d-PT, the donor concentration (3.0–7.0 at. %) is comparable to the Pb volatilization (7.0–9.0 %) necessary for liquid-phase formation in PT, as shown in Fig. 3(a) and S3. On the contrary, in d-KNN, AGG occurs with significantly lower donor concentration, approximately 0.3–0.9 at. %, compared to Na deficiency of 8–13 % [Fig. 3(a) and S3]. Namely, it is conceivable that donors may accelerate Na and K volatilization in d-KNN, while enhancing Pb deficiency in d-PT. This MV acceleration is also observed in donor-doped MgO (d-MgO) which is a metal-volatile oxide, as exhibited in Fig. 3(b). The densification and grain growth are not observed at the MgO (MD: 3.0–5.0 %) specimens sintered at 1400 °C, but the high density of 97–99 % and the large grain size of $>10 \mu\text{m}$ are found in d-MgO (donor: 0.1–0.5 at. %, MD: 8.0–12.0 %) samples. The difference between d-KNN and d-PT in terms of MD acceleration and MD enhancement is not identified in this manuscript.

3.3. Single-crystal materials grown by donor doping in KNN & PT

It is intriguing that the grain size resulting from AGG is notably large in d-KNLNS and d-KNLNSM, as shown in Fig. 7. We have previously reported that these huge grains grown by AGG are single crystals, with reaching several centimeters in size by a conventional sintering process

[47–49]. The huge grains of Fig. 7(d) are single crystals and show the excellent energy-conversion constant, $d_{33} \times g_{33}$ of $118 \cdot 10^{-12} \text{ m}^2 \text{ N}^{-1}$ and the high T_C of 390 °C as exhibited in Figs. 8 and 9. The excellent $d_{33} \times g_{33}$ is due to the huge size of grains and T_{O-T} near RT as explained above. Compared to TGG and NG, the huge grain does not have the grain boundary which degrades the piezoelectric properties, and the T_{O-T} was located at the range of 30–50 °C, in d-KNLNS and d-KNLNSM, as seen in Fig. 8.

The development of a reliable seed powder is a prerequisite for the manufacture of TGG specimens. On the contrary, this single crystal does not have any grain boundary, and thus excellent properties are guaranteed, as shown in Fig. 9. In addition, the manufacturing process is not different from that of a polycrystalline material which is the cheapest. Therefore, this single crystal which has high $d_{33} \times g_{33}$ of $118 \cdot 10^{-12} \text{ m}^2 \text{ N}^{-1}$ and T_C of 390 °C must be the next generation material for energy harvesting.

Furthermore, due to the rapid growth of grains, the single-crystal seeds were manufactured by a SMS method in both d-KNN and d-PT, as exhibited in Fig. 10 and S6. We have also previously reported the straightforward production of single-crystal seeds using a SMS method in various d-KNNs [69,70]. To date, however, the PT single-crystal seeds prepared by the SMS method have not been reported. In this manuscript, we suggest that donor doping in MVOs such as KNN and PT facilitates not only the growth of single crystals by a simple sintering process but also the fabrication of single-crystal seeds through SMS method, as seen in Figs. 7 and 10. In this study, the Ba^{2+} or Bi^{3+} ions were used as donors in KNN (A site in ABO_3 : K^+ and Na^+) and Bi^{3+} or Nb^{5+} ions were used as donors in PT and BT (A site in ABO_3 : Pb^{2+} and Ba^{2+} or B site in ABO_3 : Ti^{4+}). Fig. 11 shows the XRD patterns and SEM images of BaTiO_3 (BT) and $\text{Ba}(\text{Zr,Ti})\text{O}_3$ (BZT) seeds which are prepared by TR method. They are not metal-volatile oxides and show different sintering behaviors from d-KNN and d-PT, as seen in Figs. 5(c), 6(e–f), and S3. Moreover, the seeds are not single-crystal materials, since they were synthesized by TR. In particular, T_C (≤ 130 °C) of BT and BZT are relatively low, compared to ≥ 400 °C of PT and KNN [14,15,20,71–73]. Thus, BT and BZT frequently lose their energy harvesting performances when the energy harvesting devices operate, since the device temperature easily rises.

In the next generation of energy harvesting devices, the seed materials must show the superior performances, and the cost must be affordable [74,75]. Despite being single crystals, our proposed materials

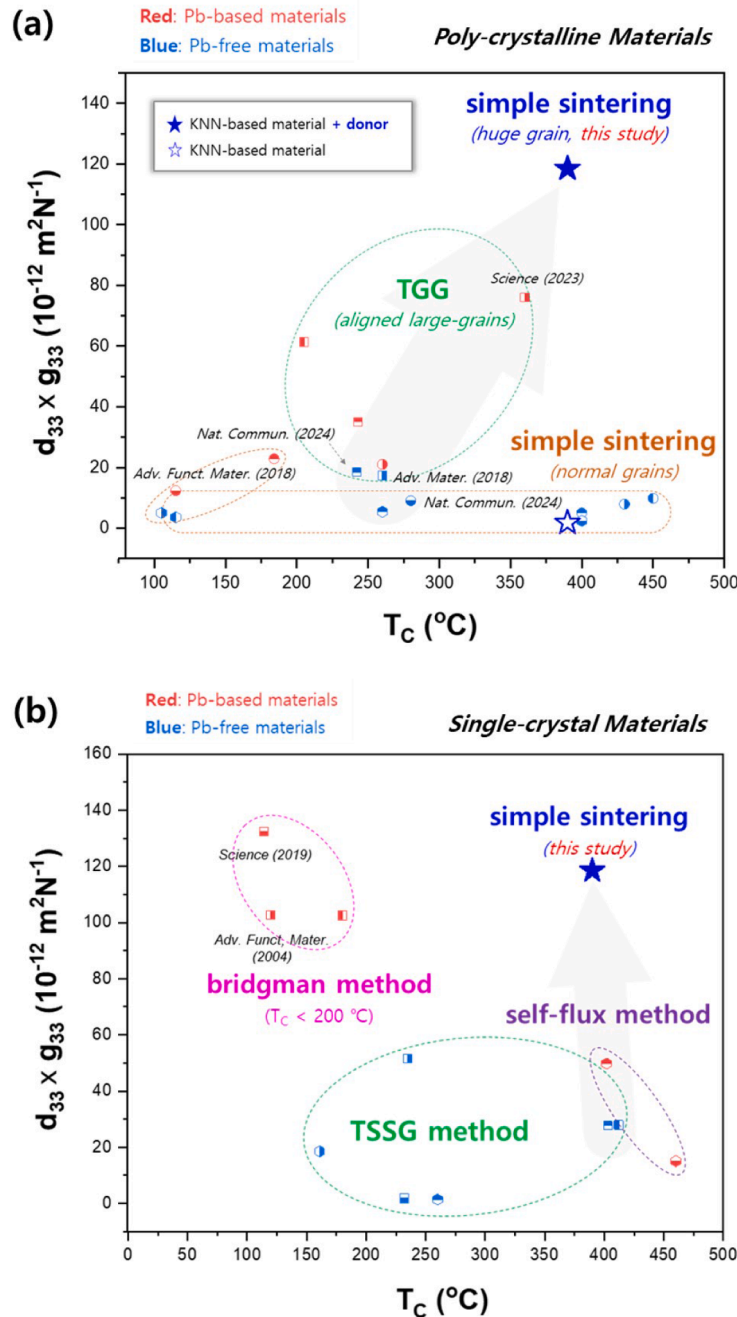


Fig. 9. Energy-conversion constants ($d_{33} \times g_{33}$) as a function of Curie temperature (T_C) in various energy harvesting materials: (a) comparison with poly-crystalline materials (TGG: templated grain growth) and (b) compared to single-crystal materials prepared with various methods (TSSG: top seed solution growth) [16,17,21–25,50–68]. $d_{33} \times g_{33}$ of $118 \cdot 10^{-12} \text{ m}^2 \text{ N}^{-1}$ and d_{33} of 1030 pC N^{-1} are observed in the huge grain of D-KNLNSM which has a high T_C of $390 \text{ }^\circ\text{C}$.

are manufactured through a cost-effective and straightforward process, making them a promising alternative to current expensive energy harvesting materials.

4. Conclusions

An excellent energy-harvesting material with high $d_{33} \times g_{33}$ of $118 \cdot 10^{-12} \text{ m}^2 \text{ N}^{-1}$ ($d_{33}=1030 \text{ pC N}^{-1}$) and T_C of $390 \text{ }^\circ\text{C}$ has been developed to effectively convert the wasted mechanical energy into electrical energy. In addition, the effects of donor doping on crystal growth behavior and physical properties in MVOs such as KNN and PT. In KNN and PT, the sintering behavior is explained by the variation of the particle surface with metal volatilization. The severe metal (Na and Pb) volatilization

was responsible for liquid phase formation at $900\text{--}1000 \text{ }^\circ\text{C}$, resulting in observed LPS at $1100 \text{ }^\circ\text{C}$. In particular, the interesting behavior is the local acceleration (or enhancement) of MV by donors in D-KNN (or D-PT), which promoted earlier localized grain growth in donor-rich regions. Consequently, AGG was more frequent in D-KNN and D-PT . AGG in D-KNN facilitated the production of single crystals with high energy-conversion constants via simple sintering processes. This crystal-growth behavior may provide significant hints for obtaining single-crystal materials prepared by simple heat-treatment in various MVOs, and thus these single-crystal materials show low cost and high performance. Furthermore, this finding can offer practical benefits in enhancing energy harvesting devices. Moreover, single-crystal seeds for next-generation energy harvesting materials were fabricated by a SMS

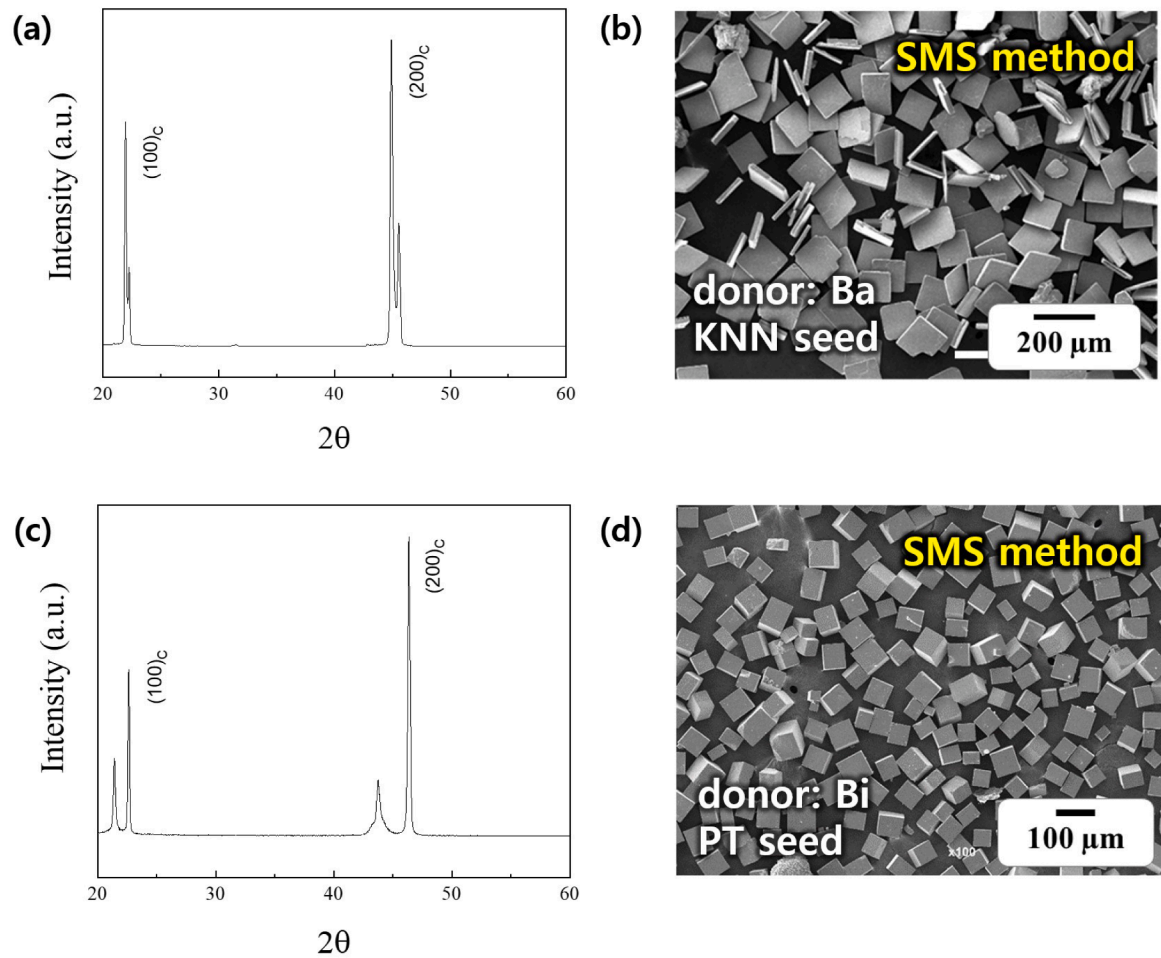


Fig. 10. X-ray diffraction (XRD) patterns and SEM images of single-crystal seeds of (a-b) D-KNN and (c-d) D-PT. They were synthesized by SMS method. The D-KNN shows orthorhombic phase and the phase of D-PT is tetragonal structure.

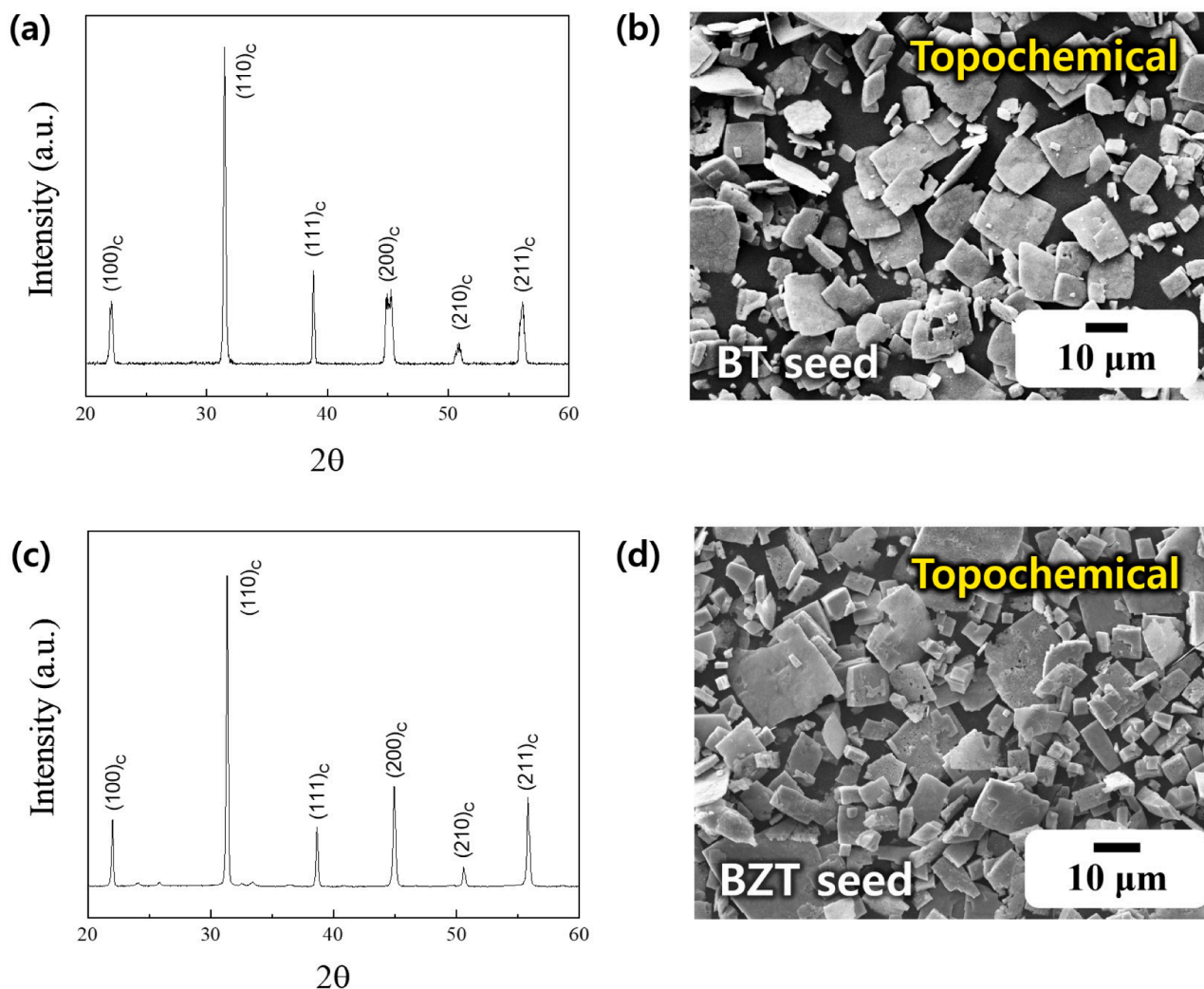


Fig. 11. X-ray diffraction (XRD) patterns and SEM images of poly-crystalline seeds of (a-b) BT and (c-d) BZT. They were synthesized by TR. Their phases are close to cubic structure.

method in D-KNN and D-PT .

CRediT authorship contribution statement

Su-Jin Ha: Writing – original draft, Investigation, Data curation, Conceptualization. **Young Kook Moon:** Investigation, Conceptualization. **Hyun-Ae Cha:** Investigation, Data curation. **Jong-Jin Choi:** Investigation, Conceptualization. **Byung-Dong Hahn:** Writing – original draft, Project administration, Funding acquisition. **Seong-Hui Choi:** Data curation. **Il-Ryeol Yoo:** Data curation. **Kyung-Hoon Cho:** Writing – original draft, Supervision, Conceptualization. **Kyoung-Seok Moon:** Writing – original draft, Conceptualization. **Cheol-Woo Ahn:** Writing – review & editing, Writing – original draft, Supervision, Project administration, Investigation, Funding acquisition, Conceptualization.

Declaration of competing interest

The authors declare that they have no known competing financial interests or personal relationships that could have appeared to influence the work reported in this paper.

Acknowledgements

This study was financially supported by the Fundamental Research

Program of the Korean Institute of Materials Science (KIMS), “Development of next-generation multifunctional-materials for breakthrough in thermal management” (Grant No. PNKA550) and Nano & Material Technology Development Program through the National Research Foundation of Korea (NRF) funded by Ministry of Science and ICT (RS-2024-00444574).

Supplementary materials

Supplementary material associated with this article can be found, in the online version, at [doi:10.1016/j.actamat.2025.121180](https://doi.org/10.1016/j.actamat.2025.121180).

References

- [1] M. Shen, K. Liu, G. Zhang, Q. Li, G. Zhang, Q. Zhang, H. Zhang, S. Jiang, Y. Chen, K. Yao, Thermoelectric coupling effect in BNT-BZT-xGaN pyroelectric ceramics for low-grade temperature-driven energy harvesting, *Nat. Commun* (2023) 7907, <https://doi.org/10.1038/s41467-023-43692-3>.
- [2] G.-T. Hwang, J. Yang, S.H. Yang, H.Y. Lee, M. Lee, D.Y. Park, J.H. Han, S.J. Lee, C. K. Jeong, J. Kim, K.-I. Park, K.J. Lee, A reconfigurable rectified flexible energy harvester via solid-State single crystal grown PMN-PZT, *Adv. Energy Mater* (2015) 1500051, <https://doi.org/10.1002/aenm.201500051>.
- [3] G.-T. Hwang, V. Annappureddy, J.H. Han, D.J. Joe, C. Baek, D.Y. Park, D.H. Kim, J. H. Park, C.K. Jeong, K.-I. Park, J.-J. Choi, D.K. Kim, J. Ryu, K.J. Lee, Self-powered wireless sensor node enabled by an Aerosol-deposited PZT flexible energy harvester, *Adv. Energy Mater* (2016) 1600237, <https://doi.org/10.1002/aenm.201600237>.

- [4] F.R. Fan, W. Tang, Z.L. Wang, Flexible nanogenerators for energy harvesting and self-powered electronics, *Adv. Mater.* (2016) 4283–4305, <https://doi.org/10.1002/adma.201504299>.
- [5] R. Hinchet, H.-J. Yoon, H. Ryu, M.-K. Kim, D.-S. Kim, S.-W. Kim, Transcutaneous ultrasound energy harvesting using capacitive triboelectric technology, *Sci.* (1979) (2019) 491–494, <https://doi.org/10.1126/science.aan3997>.
- [6] S. Kim, S.J. Choi, K. Zhao, H. Yang, G. Gobbi, S. Zhang, J. Li, Electrochemically driven mechanical energy harvesting, *Nat. Commun.* (2016) 10146, <https://doi.org/10.1038/ncomms10146>.
- [7] Y. Hu, K. Parida, H. Zhang, X. Wang, Y. Li, X. Zhou, S.A. Morris, W.H. Liew, H. Wang, T. Li, F. Jiang, M. Yang, M. Alexe, Z. Du, C.L. Gan, K. Yao, B. Xu, P.S. Lee, H.J. Fan, Bond engineering of molecular ferroelectrics renders soft and high-performance piezoelectric energy harvesting materials, *Nat. Commun.* (2022) 5607, <https://doi.org/10.1038/s41467-022-33325-6>.
- [8] Z.-X. Huang, L.-W. Li, Y.-Z. Huang, W.-X. Rao, H.-W. Jiang, J. Wang, H.-H. Zhang, H.-Z. He, J.-P. Qu, Self-poled piezoelectric polymer composites via melt-state energy implantation, *Nat. Commun.* (2024) 819, <https://doi.org/10.1038/s41467-024-45184-4>.
- [9] J. Chen, C. Zhang, R. Liu, L. Jia, Q. Niu, S. Fan, Y. Zhang, Visible periodic piezoelectric domains insilk fibroin for neurite-orientated extension, *Adv. Mater.* (2025) 2405053, <https://doi.org/10.1002/adma.202415053>.
- [10] C.R. Bowen, V. Yu. Topolov, Piezoelectric sensitivity of PbTiO₃-based ceramic/polymer composites with 0–3 and 3–3 connectivity, *Acta Mater.* (2003) 4965–4976, [https://doi.org/10.1016/S1359-6454\(03\)00341-3](https://doi.org/10.1016/S1359-6454(03)00341-3).
- [11] C.-W. Ahn, H.-C. Song, S.-H. Park, S. Nahm, K. Uchino, S. Priya, H.-G. Lee, N.-K. Kang, Low temperature sintering and piezoelectric properties in Pb(Zr_{1-x}Ti_x)O₃-Pb(Zn_{1/3}Nb_{2/3})O₃-Pb(Ni_{1/3}Nb_{2/3})O₃ ceramics, *Jpn. J. Appl. Phys.* (2005) 1314–1321, <https://doi.org/10.1143/JJAP.44.1314>.
- [12] C.-W. Ahn, S.-Y. Noh, S. Nahm, J. Ryu, K. Uchino, S.-J. Yoon, J.-S. Song, Low-temperature sintering and piezoelectric properties of ZnO-added 0.41Pb(Ni_{1/3}Nb_{2/3})O₃-0.36PbTiO₃-0.23PbZrO₃ ceramics, *Jpn. J. Appl. Phys.* (2003) 5676–5680, <https://doi.org/10.1143/JJAP.42.5676>.
- [13] C.-W. Ahn, S. Nahm, J. Ryu, K. Uchino, S.-J. Yoon, S.-J. Jung, J.-S. Song, Effects of CuO and ZnO additives on sintering temperature and piezoelectric properties of 0.41Pb(Ni_{1/3}Nb_{2/3})O₃-0.36PbTiO₃-0.23PbZrO₃ ceramics, *Jpn. J. Appl. Phys.* (2004) 205–210, <https://doi.org/10.1143/JJAP.43.205>.
- [14] V.G. Bhide, K.G. Deshmukh, M.S. Hegde, Ferroelectric properties of PbTiO₃, *Physica* (1962) 871–876, [https://doi.org/10.1016/0031-8914\(62\)90075-7](https://doi.org/10.1016/0031-8914(62)90075-7).
- [15] V.A. Chaudhari, G.K. Bichile, Synthesis, structural, and electrical properties of pure PbTiO₃ ferroelectric ceramics, *Smart Mater. Res.* (2013) 147524, <https://doi.org/10.1155/2013/147524>.
- [16] H. Tian, X. Meng, C. Hu, P. Tan, X. Cao, G. Shi, Z. Zhou, R. Zhang, Origin of giant piezoelectric effect in lead-free K_{1-x}Na_xTa_{1-y}Nb_yO₃ single crystals, *Sci. Rep.* (2016) 25637, <https://doi.org/10.1038/srep25637>.
- [17] X. Huo, L. Zheng, R. Zhang, R. Wang, J. Wang, S. Sang, Y. Wang, B. Yang, W. Cao, A high quality lead-free (Li, Ta) modified (K, Na)NbO₃ single crystal and its complete set of elastic, dielectric and piezoelectric coefficients with macroscopic 4mm symmetry, *Cryst. Eng. Comm.* (2014) 9828–9833, <https://doi.org/10.1039/C4CE01208A>.
- [18] C.-W. Ahn, D. Maurya, C.-S. Park, S. Nahm, S. Priya, A generalized rule for large piezoelectric response in perovskite oxide ceramics and its application for design of lead-free compositions, *J. Appl. Phys.* (2009) 114108, <https://doi.org/10.1063/1.3142442>.
- [19] D. Lin, K.W. Kwok, K.H. Lam, H.L.W. Chan, Structure and electrical properties of K_{0.5}Na_{0.5}NbO₃-LiSbO₃ lead-free piezoelectric ceramics, *J. Appl. Phys.* (2007) 074111, <https://doi.org/10.1063/1.2715486>.
- [20] C.-W. Ahn, C.-H. Choi, H.-Y. Park, S. Nahm, S. Priya, Dielectric and piezoelectric properties of (1–2x)(Na_{0.5}K_{0.5})NbO₃-xBaTiO₃ ceramics, *J. Mater. Sci.* (2008) 6784–6797, <https://doi.org/10.1007/s10853-008-2934-1>.
- [21] H. Leng, Y.U. Wang, Y. Yan, S.K. Karan, K. Wang, X. Li, M. Fanton, J.J. Fox, S. Priya, Water quenched and acceptor-doped textured piezoelectric ceramics for off-resonance and on-resonance devices, *Small* (2022) 2204454, <https://doi.org/10.1002/sml.202204454>.
- [22] J. Li, W. Qu, J. Daniels, H. Wu, L. Liu, J. Wu, M. Wang, S. Checchia, S. Yang, H. Lei, R. Lv, Y. Zhang, D. Wang, X. Li, X. Ding, J. Sun, Z. Xu, Y. Chang, S. Zhang, F. Li, Lead zirconate titanate ceramics with aligned crystallite grains, *Sci.* (1979) (2023) 87–93, <https://doi.org/10.1126/science.adf6161>.
- [23] P. Li, J. Zhai, B. Shen, S. Zhang, X. Li, F. Zhu, X. Zhang, Ultrahigh piezoelectric properties in textured (K,Na)NbO₃-based lead-free ceramics, *Adv. Mater.* (2018) 1705171, <https://doi.org/10.1002/adma.201705171>.
- [24] J. Lin, J. Qian, G. Ge, Y. Yang, J. Li, X. Wu, G. Li, S. Wang, Y. Liu, J. Zhang, J. Zhai, X. Shi, H. Wu, Multiscale reconfiguration induced highly saturated poling in lead-free piezoceramics for giant energy conversion, *Nat. Commun.* (2024) 2560, <https://doi.org/10.1038/s41467-024-46894-5>.
- [25] Y. Chang, J. Wu, Z. Liu, E. Sun, L. Liu, Q. Kou, F. Li, B. Yang, W. Cao, Grain-oriented ferroelectric ceramics with single-crystal-like piezoelectric properties and low texture temperature, *ACS Appl. Mater. Interfaces* (2020) 38415–38424, <https://doi.org/10.1021/acsmi.0c11680>.
- [26] C.K. Jeong, K.-I. Park, J. Ryu, G.-T. Hwang, K.J. Lee, Large-area and flexible lead-free nanocomposite generator using alkaline niobate particles and metal nanorod filler, *Adv. Funct. Mater.* (2014) 2620–2629, <https://doi.org/10.1002/adfm.201303484>.
- [27] J. An, H. Park, Y.H. Jung, S. Min, D.H. Kim, D.J. Joe, S.-G. Lee, D.Y. Hyeon, Y. Je, H.-S. Seo, et al., In vivo flexible energy harvesting on porcine heart via highly-piezoelectric PIN–PMN–PT single crystal, *Nano Energy* (2024) 109227, <https://doi.org/10.1016/j.nanoen.2023.109227>.
- [28] Y. Liu, Y. Zhang, Z. Yang, H. Ye, J. Feng, Z. Xu, X. Zhang, R. Munir, J. Liu, P. Zuo, et al., Multi-inch single-crystalline perovskite membrane for high-detectivity flexible photosensors, *Nat. Commun.* (2018) 5302, <https://doi.org/10.1038/s41467-018-07440-2>.
- [29] F. Kang, B. Yao, W. Zhang, F. Yao, Q. Zhao, L. Miao, F. Zhao, Z. Huang, W. Zhao, G. A. Sevvardi, et al., In situ topochemically converted 2D BaTiO₃ polycrystals with multifarious zone axes, *Mater. Adv.* (2022) 4878–4889, <https://doi.org/10.1039/D2MA00283C>.
- [30] S.F. Poterala, R.J. Meyer Jr., G.L. Messing, Low-field dynamic magnetic alignment and templated grain growth of diamagnetic PMN–PT ceramics, *J. Mater. Res.* (2013) 2960–2969, <https://doi.org/10.1557/jmr.2013.303>.
- [31] Y. Chang, H. Ning, J. Wu, S. Zhang, T. Lü, B. Yang, W. Cao, Formation mechanism of (001) oriented perovskite SrTiO₃ microplatelets synthesized by topochemical microcrystal conversion, *Inorg. Chem.* (2014) 11060–11067, <https://doi.org/10.1021/ic501604c>.
- [32] C.-W. Ahn, H.-Y. Lee, G. Han, S. Zhang, S.-Y. Choi, J.-J. Choi, J.-W. Kim, W.-H. Yoon, J.-H. Choi, D.-S. Park, et al., Self-growth of centimeter-scale single crystals by normal sintering process in modified potassium sodium niobate ceramics, *Sci. Rep.* (2015) 17656, <https://doi.org/10.1038/srep17656>.
- [33] Z. Cen, S. Bian, Z. Xu, K. Wang, L. Guo, L. Li, X. Wang, Simultaneously improving piezoelectric properties and temperature stability of Na_{0.5}K_{0.5}NbO₃ (KNN)-based ceramics sintered in reducing atmosphere, *J. Adv. Ceram.* (2021) 820–831, <https://doi.org/10.1007/s40145-021-0475-0>.
- [34] S.-Y. Choi, D.-Y. Yoon, S.-J.L. Kang, Kinetic formation and thickening of intergranular amorphous films at grain boundaries in barium titanate, *Acta Mater.* (2004) 3721–3726, <https://doi.org/10.1016/j.actamat.2004.04.026>.
- [35] S.J. Zheng, X.L. Ma, T. Yamamoto, Y. Ikuhara, Layer-by-layer assembled nanowire networks enable graph-theoretical design of multifunctional coatings, *Acta Mater.* (2013) 2298–2307, <https://doi.org/10.7302/23mt-jr71>.
- [36] C.-W. Ahn, H.-Y. Park, S. Nahm, K. Uchino, H.-G. Lee, H.-J. Lee, Structural variation and piezoelectric properties of 0.95(Na_{0.5}K_{0.5})NbO₃-0.05BaTiO₃ ceramics, *Sens. Actuators A* (2007) 255–260, <https://doi.org/10.1016/j.sna.2006.10.036>.
- [37] C.-W. Ahn, C.-S. Park, C.-H. Choi, S. Nahm, M.-J. Yoo, H.-G. Lee, S. Priya, Sintering behavior of lead-free (K,Na)NbO₃-based piezoelectric ceramics, *J. Am. Ceram. Soc.* (2009) 2033–2038, <https://doi.org/10.1111/j.1551-2916.2009.03167.x>.
- [38] J. Liu, A. Lal, R.M. German, Densification and shape retention in supersolidus liquid phase sintering, *Acta Mater.* (1999) 4615–4626, [https://doi.org/10.1016/S1359-6454\(99\)00320-1](https://doi.org/10.1016/S1359-6454(99)00320-1).
- [39] P. Zhou, F. Yu, X. Zeng, M. Gao, C. Zhao, C. Lin, T. Lin, L. Luo, J. Lin, X. Wu, Phase transition monitoring and temperature sensing via FIR technology in Bi/Sm-codoped KNN transparent ceramics, *J. Am. Ceram. Soc.* (2023) 1648–1656, <https://doi.org/10.1111/jace.19344>.
- [40] H.-S. Kim, J.-S. An, H.B. Bae, S.-Y. Chung, Atomic-scale observation of premelting at 2D lattice defects inside oxide crystals, *Nat. Commun.* (2023) 2255, <https://doi.org/10.1038/s41467-023-37977-w>.
- [41] S.-C. Jeon, S.-Y. Kim, K.-S. Moon, Interface structure dependent step free energy and grain growth behavior of core/shell grains in (Y, Mg)-doped BaTiO₃ containing a liquid phase, *J. Eur. Ceram. Soc.* (2022) 2804–2812, <https://doi.org/10.1016/j.jeurceramsoc.2022.01.045>.
- [42] S.-J.L. Kang, M.-G. Lee, S.-M. An, Microstructural evolution during sintering with control of the interface structure, *J. Am. Ceram. Soc.* (2009) 1464–1471, <https://doi.org/10.1111/j.1551-2916.2009.03106.x>.
- [43] W. Jo, D.-Y. Kim, N.-M. Hwang, Effect of interface structure on the microstructural evolution of ceramics, *J. Am. Ceram. Soc.* (2006) 2369–2380, <https://doi.org/10.1111/j.1551-2916.2006.01160.x>.
- [44] C.E. Seo, D.Y. Yoon, The effect of MgO addition on grain growth in PMN–35PT, *J. Am. Ceram. Soc.* (2005) 963–967, <https://doi.org/10.1111/j.1551-2916.2005.00213.x>.
- [45] Z. Cen, Y. Yu, P. Zhao, L. Chen, C. Zhu, L. Li, X. Wang, Grain configuration effect on the phase transition, piezoelectric strain, and temperature stability of KNN-based ceramics, *Mater. Chem. C* (2019) 1379–1387, <https://doi.org/10.1039/C8TC05253K>.
- [46] W. Liu, H. Wang, W. Hu, Y. Du, C. Cheng, Understanding the origin of the high piezoelectric performance of KNN-based ceramics from the perspective of lattice distortion, *Ceram. Int.* (2022) 9731–9738, <https://doi.org/10.1016/j.ceramint.2021.12.174>.
- [47] A. Rahman, K.-H. Cho, C.-W. Ahn, J. Ryu, J.-J. Choi, J.-W. Kim, W.-H. Yoon, J.-H. Choi, D.-S. Park, B.-D. Hahn, et al., A composition design rule for crystal growth of centimeter scale by normal sintering process in modified potassium sodium niobate ceramics, *J. Eur. Ceram. Soc.* (2018) 1416–1420, <https://doi.org/10.1016/j.jeurceramsoc.2017.11.028>.
- [48] J.G. Fisher, S.-H. Sim, T.T. Doan, E. Uwiragiye, J. Mok, J. Lee, Comparison of (K_{0.5}Na_{0.5})NbO₃ single crystals grown by seed-free and seeded solid-state single crystal growth, *Mater.* (2023) 3638, <https://doi.org/10.3390/ma16103638>.
- [49] C.-W. Ahn, A. Rahman, J. Ryu, J.-J. Choi, J.-W. Kim, W.-H. Yoon, J.-H. Choi, D.-S. Park, B.-D. Hahn, et al., Composition design for growth of single crystal by abnormal grain growth in modified potassium sodium niobate ceramics, *Cryst. Growth Des.* (2016) 6586–6592, <https://doi.org/10.1021/acs.cgd.6b01287>.
- [50] C.-W. Ahn, M. Karmarkar, D. Viehland, D.-H. Kang, K.-S. Bae, S. Priya, Low-temperature sintering and piezoelectric properties of CuO-doped (K_{0.5}Na_{0.5})NbO₃ ceramics, *Ferroelectr. Lett.* (2008) 66–72, <https://doi.org/10.1080/07315170802353058>.
- [51] T.R. Shrobt, S.J. Zhang, Lead-free piezoelectric ceramics: alternatives for PZT? *J. Electroceram.* (2007) 113–126, <https://doi.org/10.1007/s10832-007-9095-5>.

- [52] J. Zou, M. Song, X. Zhou, W. Chi, T. Wei, K. Zhou, D. Zhang, S. Zhang, Enhancing piezoelectric coefficient and thermal stability in lead-free piezoceramics: insights at the atomic-scale, *Nat. Commun.* (2024) 8591, <https://doi.org/10.5061/dryad.zs7h444jk1>.
- [53] H. Du, F. Tang, D. Liu, D. Zhu, W. Zhou, S. Qu, The microstructure and ferroelectric properties of $(K_{0.5}Na_{0.5})NbO_3$ - $LiNbO_3$ lead-free piezoelectric ceramics, *Mater. Sci. Eng. B* 136 (2007) 165–169, <https://doi.org/10.1016/j.mseb.2006.09.031>.
- [54] Y. Huan, X. Wang, W. Yang, L. Hou, M. Zheng, T. Wei, X. Wang, Optimizing energy harvesting performance by tailoring ferroelectric/relaxor behavior in KNN-based piezoceramics, *J. Adv. Ceram.* (2022) 935–944, <https://doi.org/10.1007/s40145-022-0587-1>.
- [55] Q. Guo, F. Li, F. Xia, X. Gao, P. Wang, H. Hao, H. Sun, H. Liu, S. Zhang, High-performance Sm-doped $Pb(Mg_{1/3}Nb_{2/3})O_3$ - $PbZrO_3$ - $PbTiO_3$ -based piezoceramics, *ACS. Appl. Mater. Interfaces* (2019) 43359–43367, <https://doi.org/10.1021/acsami.9b15424>.
- [56] D. Yuan, Y. Yang, Q. Hu, Y. Wang, Structures and properties of $Pb(Zr_{0.5}Ti_{0.5})O_3$ - $Pb(Zn_{1/3}Nb_{2/3})O_3$ - $Pb(Ni_{1/3}Nb_{2/3})O_3$ ceramics for energy harvesting devices, *J. Am. Ceram. Soc.* (2014) 3719–4059, <https://doi.org/10.1111/jace.13175>.
- [57] V. Bijalwan, J. Erhart, Z. Spatz, D. Sobola, V. Prajzler, P. Tofel, K. Maca, Composition driven $(Ba,Ca)(Zr,Ti)O_3$ lead-free ceramics with large quality factor and energy harvesting characteristics, *J. Am. Ceram. Soc.* (2021) 655–1187, <https://doi.org/10.1111/jace.17497>.
- [58] X. Gao, J. Wu, Y. Yu, Z. Chu, H. Shi, S. Dong, Giant piezoelectric coefficients in relaxor piezoelectric ceramic PNN-PZT for vibration energy harvesting, *Adv. Funct. Mater.* (2018) 1706895, <https://doi.org/10.1002/adfm.201706895>.
- [59] C. Qiu, B. Wang, N. Zhang, S. Zhang, J. Liu, D. Walker, Y. Wang, H. Tian, T. R. Shrout, Z. Xu, et al., Transparent ferroelectric crystals with ultrahigh piezoelectricity, *Nature* (2020) 350–354, <https://doi.org/10.1145/2792745.2792775>.
- [60] F. Li, M.J. Cabral, B. Xu, Z. Cheng, E.C. Dickey, J.M. LeBeau, J. Wang, J. Luo, S. Taylor, S. Zhang, Giant piezoelectricity of Sm-doped $Pb(Mg_{1/3}Nb_{2/3})O_3$ - $PbTiO_3$ single crystals, *Sci.* (1979) (2019) 264–268, <https://doi.org/10.1126/science.aaw2781>.
- [61] C. Luo, T. Karaki, Z. Wang, Y. Sun, Y. Yamashita, J. Xu, High piezoelectricity after field cooling AC poling in temperature-stable ternary single crystals manufactured by continuous-feeding Bridgman method, *J. Adv. Ceram.* (2022) 57–65, <https://doi.org/10.1007/s40145-021-0490-1>.
- [62] B.-J. Fang, Y.-J. Shan, H.-Q. Xu, H.-S. Luo, Z.-W. Yin, On the feasibility of growing $Pb[(Zn_{1/3}Nb_{2/3})_{0.91}Ti_{0.09}]O_3$ single crystals, *Adv. Funct. Mater.* (2004) 103–190, <https://doi.org/10.1002/adfm.200304491>.
- [63] L. Zheng, S. Li, S. Sang, J. Wang, X. Huo, R. Wang, Z. Yuan, W. Cao, Complete set of material constants of single domain $(K, Na)(Nb, Ta)O_3$ single crystal and their orientation dependence, *Appl. Phys. Lett.* (2014) 212902, <https://doi.org/10.1063/1.4902548>.
- [64] H. Zhou, H. Deng, X. Liu, H. Yan, X. Zhao, H. Luo, J. Xu, Dielectric and piezoelectric properties of lead-free $(K_{0.44}Na_{0.46})NbO_3$ -0.5 % MnO_2 single crystals grown by the TSSG method, *Ceram. Int.* (2016) 15327–15331, <https://doi.org/10.1016/j.ceramint.2016.06.174>.
- [65] X. Huo, R. Zhang, L. Zheng, S. Zhang, R. Wang, J. Wang, S. Sang, B. Yang, W. Cao, $(K, Na, Li)(Nb, Ta)O_3$:mn lead-free single crystal with high piezoelectric properties, *J. Am. Ceram. Soc.* (2015) 1829–1835, <https://doi.org/10.1111/jace.13540>.
- [66] M. Jiang, J. Zhang, G. Rao, D. Li, C.A. Randall, T. Li, B.L. Peng, L. Li, Z. Gu, X. Liu, et al., Ultrahigh piezoelectric coefficient of a lead-free $K_{0.5}Na_{0.5}NbO_3$ -based single crystal fabricated by a simple seed-free solid-state growth method, *J. Mater. Chem. C* (2019) 14845–14854, <https://doi.org/10.1039/C9TC05143K>.
- [67] S. Zhang, L. Lebrun, S. Rhee, R.E. Eitel, C.A. Randall, T.R. Shrout, Crystal growth and characterization of new high Curie temperature $(1-x)BiScO_3$ - $xPbTiO_3$ single crystals, *J. Cryst. Growth* (2002) 210–216, [https://doi.org/10.1016/S0022-0248\(01\)02093-0](https://doi.org/10.1016/S0022-0248(01)02093-0).
- [68] S. Zhang, C.A. Randall, T.R. Shrout, Characterization of perovskite piezoelectric single crystals of $0.43BiScO_3$ - $0.57PbTiO_3$ with high Curie temperature, *J. Appl. Phys.* (2004) 4291–4295, <https://doi.org/10.1063/1.1682694>.
- [69] S. Park, H. Choi, G.-T. Hwang, M. Peddigari, C.-W. Ahn, B.-D. Hahn, W.-H. Yoon, J. W. Lee, K.I. Park, J.M. Jang, et al., Molten-salt processed potassium sodium niobate single-crystal microcuboids with dislocation-induced nanodomain structures and relaxor ferroelectric behavior, *ACS. Nano* (2022) 15328–15338, <https://doi.org/10.1021/acsnano.2c06919>.
- [70] S. Park, A. Rahman, Y. Min, G.-T. Hwang, J.-J. Choi, B.-D. Hahn, K.-H. Cho, J. W. Lee, S. Nahm, C.-W. Ahn, An easy approach to obtain textured microstructure and transparent seed crystal prepared by simple molten salt synthesis in modified potassium sodium niobate, *J. Eur. Ceram. Soc.* (2020) 1232–1235, <https://doi.org/10.1016/j.jeurceramsoc.2019.11.007>.
- [71] H. Lemziouka, L. El Hachimi Omari, R. Moubah, A. Boutahar, S. Bahhar, M. Abid, H. Lassri, Structural, dielectric, and optical properties of Cu-doped $PbTiO_3$ ceramics prepared by sol-gel, *Mater. Today Proc.* (2021) 3940–3945, <https://doi.org/10.1016/j.matpr.2020.09.094>.
- [72] Z. Lv, J. Wei, T. Yang, Z. Sun, Z. Xu, Manipulation of Curie temperature and ferroelectric polarization for large electrocaloric strength in $BaTiO_3$ -based ceramics, *Ceram. Int.* (2020) 14978–14984, <https://doi.org/10.1016/j.ceramint.2020.03.027>.
- [73] S.M. Neirman, The Curie point temperature of $Ba(Ti_{1-x}Zr_x)O_3$ solid solutions, *J. Mater. Sci.* (1988) 3973–3980, <https://doi.org/10.1007/BF01106823>.
- [74] E. Im, S. Park, G.-T. Hwang, D.C. Hyun, Y. Min, G.D. Moon, Single-crystal ferroelectric-based $(K,Na)NbO_3$ microcuboid/CuO nanodot heterostructures with enhanced photo-piezocatalytic activity, *Small* (2024) 2304360, <https://doi.org/10.1002/smll.202304360>.
- [75] G. Huangfu, K. Zeng, B. Wang, J. Wang, Z. Fu, F. Xu, S. Zhang, H. Luo, D. Viehland, Y. Guo, Giant electric field-induced strain in lead-free piezoceramics, *Sci.* (1979) (2022) 1125–1130, <https://doi.org/10.1126/science.ade2964>.